J. Fluid Mech. (1999), *vol.* 395, *pp.* 1–28. Printed in the United Kingdom

Aeroacoustic properties of supersonic elliptic jets

By KEVIN W. KINZIE[1] AND DENNIS K. McLAUGHLIN[2]

[1] General Electric Aircraft Engines, One Neumann Way, MD A410, Cincinnati, OH 45215, USA

[2] Department of Aerospace Engineering, The Pennsylvania State University, University Park, PA 16802, USA

(Received 3 February 1998 and in revised form 29 March 1999)

The aerodynamic and acoustic properties of supersonic elliptic and circular jets are experimentally investigated. The jets are perfectly expanded with an exit Mach number of approximately 1.5 and are operated in the Reynolds number range of 25 000 to 50 000. The reduced Reynolds number facilitates the use of conventional hot-wire anemometry and a glow discharge excitation technique which preferentially excites the varicose or flapping modes in the jets. In order to simulate the high-velocity and low-density effects of heated jets, helium is mixed with the air jets. This allows the large-scale structures in the jet shear layer to achieve a high enough convective velocity to radiate noise through the Mach wave emission process.

Experiments in the present work focus on comparisons between the cold and simulated heated jet conditions and on the beneficial aeroacoustic properties of the elliptic jet. When helium is added to the jet, the instability wave phase velocity is found to approach or exceed the ambient sound speed. The radiated noise is also louder and directed at a higher angle from the jet axis. In addition, near-field hot-wire spectra are found to match the far-field acoustic spectra only for the helium/air mixture case. These results demonstrate that there are significant differences between unheated and heated asymmetric jets in the Mach 1.5 speed range, many of which have been found previously for circular jets. The elliptic jet was also found to radiate less noise than the round jet at comparable operating conditions.

1. Introduction

1.1. *Overview*

Beginning with the work of Crow & Champagne (1971), Tam (1975), and Morris & Tam (1979), it became well known that the dynamics of large-scale vortical structures play an important role in the development of free shear flows. McLaughlin, Morrison & Troutt (1975), Morrison & McLaughlin (1979), and Troutt & McLaughlin (1982) showed how the large-scale structures in low-to-moderate Reynolds number supersonic jets are a direct source of noise. Their work, along with the work of Seiner, McLaughlin & Liu (1982), showed that, when scaled properly, the noise radiated from the lower Reynolds number supersonic axisymmetric jets is very similar in frequency content and directivity to the high Reynolds number jets. Analytical work by Morris & Tam (1979) and Tam & Burton (1984) modelled the large-scale structures in a supersonic axisymmetric jet as instability waves. By using quasi-linear stability methods, they predicted the noise radiated by the instability waves. A major aspect

of the analytical jet noise models of Tam & Morris is that the calculations of the flow fluctuation properties (the noise generators) can be compared directly with experiment. This is in contradistinction to the quadruple noise generators that form the foundation of the original Lighthill (1952) theory. The quadruple formulation of the flow fluctuations is so complicated, that to date no one has successfully modelled them (analytically) or measured them (experimentally).

An excellent example of the verification of analytically modelled noise generators involved the work of Tam & Burton (1984) in demonstrating good agreement when making direct comparisons of the predicted wave properties and radiated sound with the experimental measurements of Troutt & McLaughlin (1982). As may be inferred from the analysis of Ffowcs Williams (1963), when the convection velocity of the turbulence structures is supersonic, the noise radiated from them dominates the sound field. All of this information indicates that an understanding of supersonic jet noise requires a firm understanding of the large-scale turbulent structures in the jet.

With the interest in the design of a more viable generation of supersonic transport aircraft, the topic of supersonic jet noise has received much attention in recent years. Improved methods of jet noise suppression must be developed in order to reduce the noise radiated from the propulsion system to acceptable levels. One promising method of noise reduction is the use of jets with non-circular exit geometries. Non-circular exit geometries have a distinct advantage over many other noise suppression devices in that they incur very little performance loss. The asymmetry in the non-circular jet flow promotes a more rapid mixing of the jet plume with the ambient air, which leads to a faster deceleration of the flow compared to that of a circular jet. Since the noise from supersonic jets is a strong function of velocity, it is advantageous to reduce the jet velocity as quickly as possible. In particular, if the region over which the large-scale turbulent structures possess supersonic phase speeds can be shortened, there is the possibility for significant noise reduction. The disadvantage of non-circular jet geometries is that they result in a more complex nozzle and flow field than round jets. Additionally, theoretical analysis and experimental measurements also become more complex and difficult.

Seiner & Ponton (1991) and Seiner *et al.* (1992) performed experiments with rectangular, elliptical, and circular supersonic jets. Their findings showed that the non-circular geometries are able to provide noise reduction over the circular case, particularly when the noise generation is dominated by Mach wave radiation. Kantola (1979) made measurements in heated subsonic jets and showed that the sound power from a rectangular jet is up to 3 dB less than that from a circular jet. Even in heated subsonic flows, the turbulent structures can achieve convective Mach numbers exceeding unity resulting in Mach wave radiation. There was also a definite 'loud' and 'quiet' plane measured by Seiner & Ponton (1991) and Seiner *et al.* (1992) in the elliptic jet and by Kantola in the rectangular jet. This phenomenon could be exploited in an engine application by directing the 'quiet' plane in the direction most sensitive to noise radiation.

Compared with the experiments, fewer analytical and computational studies focusing on shock-free supersonic non-circular jets have been performed. Morris & Bhat (1992, 1993, 1995) have extended the stability analysis procedure for axisymmetric jets to predict the noise from elliptic jets. By using an elliptic cylindrical coordinate system, they solved an 'inner' flow solution from the compressible Rayleigh equation and matched it with an 'outer' acoustic solution to solve both the near and far pressure fields. As will be mentioned throughout this manuscript, comparisons of their work with the experiments reported here show good agreement.

1.2. *Heated jet research*

In unheated jets at low supersonic Mach numbers, the large-scale turbulent structures typically do not achieve a supersonic phase speed. Morrison & McLaughlin (1979) measured the phase speed of the dominant jet Strouhal number component to be only about three-quarters of the ambient sound speed for a cold Mach 1.5 circular jet. This indicates that the radiated noise from such a jet would not contain Mach wave emission. However when a Mach 1.5 jet is heated, the jet velocity and the turbulent structure convection velocity increase significantly. In most practical applications, such as turbojet engine exhausts, the jet static temperature is well above the ambient temperature.

There are relatively few experimental investigations of heated supersonic jet noise. Tanna, Dean & Fisher (1975) performed experiments which attempted to isolate the effect of temperature changes on jet noise (while holding the jet velocity constant). They found that at low jet exit velocities, increasing temperature increased the radiated noise, particularly at the lower frequencies. However, at high jet velocities, increasing the temperature reduced the radiated noise over all frequencies. This was attributed to the different dependences on jet temperature and velocity of the two major noise sources in the jet. These sources are the turbulent mixing noise and density/temperature fluctuations. The latter source dominates the noise at low velocities and high temperatures while the former dominates at higher velocities.

Lau (1981) investigated the effects of Mach number and temperature on the mean flow and turbulence characteristics in round jets. He reported for a Mach 1.4 jet that heating made only small changes in the jet spread rate until about $T_j/T_0 = 1.6$ at which point the spread rate increased. He also measured a contraction in the length of the jet potential core as the jet was heated.

More recently, Seiner *et al.* (1992) measured the effects of temperature on supersonic jet noise emission. They found that as the jet was heated, the spectral characteristics and directivity of the radiated noise was consistent with the concept of Mach wave emission. They also observed a decrease in the growth rate of the jet shear layer through the potential core region as the temperature increased, accompanied by a decrease in the potential core length. The discrepancy in the shear layer growth rate observations between Lau (1981) and Seiner *et al.* (1992) is not fully understood. It is likely related to the different methods each used to characterize the shear layer growth rate. In the area of numerical modelling, Tam & Chen (1994) extended the analysis of Tam & Burton (1984) to include a stochastic model of the instability waves to predict the turbulent jet mixing noise of Seiner *et al.* (1992). The calculated directivities showed good agreement with the measurements.

All of this research points to the conclusion that there are significant differences in how heated moderately supersonic jets generate noise in comparison with their unheated counterparts. Therefore, in order to study jets under realistic engine operating conditions, they should be heated so that the convection velocity of the structures is supersonic and the effects of Mach wave radiation can be measured. Because the jet noise facility at Penn State is not equipped to operate heated jets, the low density and high velocity of hot jets are simulated by using a lower density gas with different properties than air, namely helium. This allows the jet properties to be compared as the operating conditions change from cold to simulated hot conditions and to observe the effects of the simulated jet heating on the jet flow structure and radiated sound field. While there are some differences between an actual heated jet and the

simulation due to the dissimilar ratio of specific heats, the simulation closely matches the operating conditions of a hot jet. The primary noise generation mechanism found in heated jets, Mach wave emission, is also present in the current simulation.

There are two major objectives of the present work:

(i) To investigate the aeroacoustics properties of an elliptic Mach 1.5 near-perfectly expanded supersonic jet as the simulated jet temperature is increased using a helium/air mixture as the jet working gas.

(ii) To establish an experimental data base of acoustic and flow fluctuation measurements most relevant to the dominant noise generation processes for use in current and future computational and analytical prediction methods of non-circular supersonic jets.

These objectives are achieved by making measurements of the mean and fluctuating jet flow-field properties and relating those to the measured acoustic properties of the jet. All measurements are made under pure air conditions or with a helium/air mixture to simulate a heated jet with an approximate jet-to-ambient temperature ratio of 1.2. Thus, results from experiments conducted at the two operating conditions can be directly compared.

2. Experimental details

2.1. *Technical approach*

The experiments reported here were performed in the anechoic low-pressure jet noise facility at The Pennsylvania State University. Although operation at reduced Reynolds number does result in an inexact simulation there are several benefits that are realized from this approach that allow the investigation to complement other conventional experiments. Typical Reynolds numbers for these experiments are 25 000 to 50 000 based upon jet exit diameter, D_{eq}, which compares to 2×10^6 for conventional model round jet experiments as reported in Seiner *et al.* (1992). Under these conditions, the large-scale structures in the jet, which are the primary noise generators in this Mach number range, are easier to quantify as viscous forces reduce the small-scale turbulence structure. As a result, the lower Reynolds number jets allow a good comparison to the instability wave models like that of Morris & Bhat (1992, 1993, 1995). Since these models identify such quantities as the most unstable frequency components and the individual modal content information, the lower Reynolds number jets make the evaluation of these models easier. The reduced Reynolds number jets have been demonstrated to possess aerodynamic and acoustic properties similar to their higher Reynolds number counterparts (Troutt & McLaughlin 1982; Seiner *et al.* 1982), since the large-scale structures are relatively unaffected by the Reynolds number and they are the dominant noise generators of supersonic jets.

The reduced Reynolds number condition is achieved by exhausting the jets into the low-pressure environment of the jet noise facility anechoic chamber. Chamber pressures of around 1/20th of an atmosphere are common. As a result, the low dynamic pressure of the jet flow allows standard hot-wire anemometry to be used without the typical problems of wire breakage in supersonic flow. Also, the low ambient pressure allows the use of an oscillating glow discharge excitation system. The glow discharge allows different instability modes to be excited in the jets and provides a phase reference for the microphone and hot-wire signals. This degree of active control over the jet is a significant advantage in research on supersonic jet noise.

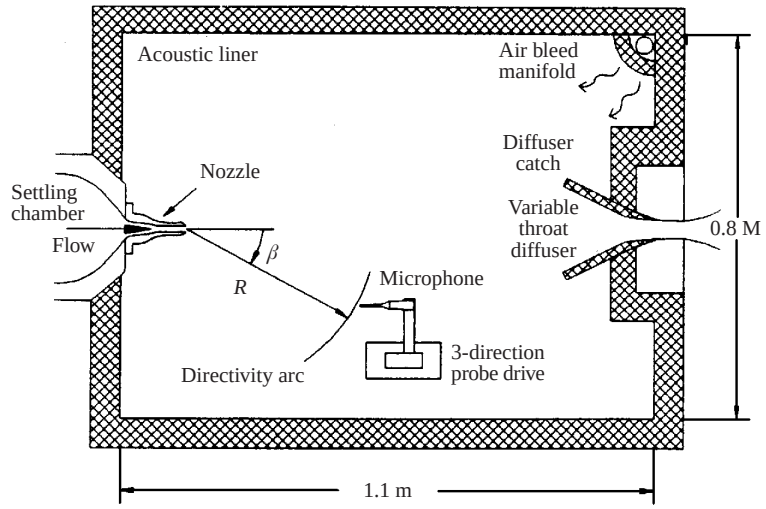

FIGURE 1. Facility anechoic chamber.

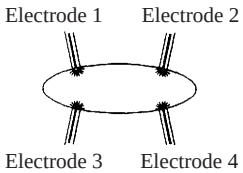

FIGURE 2. Glow discharge electrode orientation.

2.2. *Facility description*

A schematic of the jet noise anechoic chamber is shown in figure 1. Its dimensions are $0.7 \times 0.8 \times 1.1$ m, and it is lined with acoustic foam 5 cm thick which produces an effectively anechoic environment for frequencies above 1 kHz. The elliptic nozzle used for this research has an aspect ratio of 3 : 1 and is designed for shock-free flow with a nominal exit Mach number of 1.5. The nozzle exit has a major axis length of 24 mm and a minor axis length of 8 mm. The exit area of the nozzle is 151 mm^2, which is equivalent to an axisymmetric nozzle with diameter $D_{eq} = 13.8$ mm. The equivalent diameter, D_{eq}, is used as the length scale for non-dimensionalizing the experimental results. While other length scales could be chosen, non-dimensionalizing by the equivalent area diameter allows the elliptic and circular jets to be compared based on mass flow and thrust since equivalent area jets will produce approximately the same mass flow and thrust for the same flow conditions. Note that the jet aspect ratio will undoubtedly influence the jet development and the choice of length-scaling parameters for the elliptic jet could affect the interpretation of the results. Therefore, when comparing results from non-circular jets, care must be taken to ensure that the choice of length scales is appropriate to the specific application.

The round nozzle tested is also designed to be shock-free at a Mach number of 1.5 and has a diameter of 10 mm and exit area of 78.5 mm^2. The elliptic nozzle is fitted with four glow discharge electrodes oriented as shown in figure 2. The electrodes are located at azimuthal angles of approximately 45°, 135°, 225°, and 315° in an

elliptic cylindrical coordinate (ECC) system. Although the gas temperature within the glow discharge is several thousand degrees Kelvin, the residual temperature increase of the gas that passes through the glow has been measured to be negligible. Since the electrodes are located just outside the nozzle exit, very close to the flow, the modulating local high temperature perturbs the jet shear layer at the chosen frequency with minimal disturbance to the jet flow.

Each electrode can be individually controlled and therefore different instability modes can be preferentially excited in the jet. For instance, by modulating all four electrodes in phase, a varicose instability can be excited. The varicose mode is equivalent to an axisymmetric mode in a circular jet. By exciting electrodes 1 and 2 exactly 180° out of phase from electrodes 3 and 4 (see figure 2), a flapping mode about the major axis (flapping in the minor-axis plane) can be excited. Other combinations will lead to the excitation of other modes in the jet. The ability to excite specific modes in the jet is a valuable tool in research on supersonic jets. It should be noted that while the predominant mode of excitation can be selected, the excitation actually results in somewhat of multi-mode mix due to the point nature of the electrodes.

Flow-field fluctuation measurements were made with a Disa Model 55D01 constant-temperature hot-wire anemometer system. The probes consisted of Disa Model 55A53 sub-miniature probes epoxied to the upper edge of a slender brass wedge. The frequency response of the probes is in excess of 45 kHz which exceeds the required frequency range for these experiments. Calibration of the hot wires is a rather involved process described in detail in Kinzie (1995). In summary, the process involves recording the anemometer mean voltage with the hot wire located in the potential core region of a Mach 1.5 round jet for a wide range of jet mass velocities (ρu) and helium concentrations (c). From the curve fits of the data, the influence coefficients of the response of the hot wires to the two parameters ρu and c are established, and the local linearization method first developed by Kovasznay (1950) is adapted to the gas mixture jets.

Acoustic measurements were made with 1/8 in. diameter condenser microphones. Following the work of Troutt & McLaughlin (1982) and Morrison & McLaughlin (1979), the sound pressure level is calculated using a reference pressure, p_{ref}, scaled by the ratio of atmospheric pressure, p_{atm}, and ambient chamber pressure, p_{ch}, as follows:

$$SPL = 20 \log_{10}[p_{rms}/p_{ref}],$$

where

$$p_{ref} = [p_{ch}/p_{atm}](20 \times 10^6)\,\mathrm{N\,m^{-2}}$$

where p_{rms} is the root-mean-square pressure.

Figure 3 shows a diagram of the coordinate system and measurement plane notation used for this research. The major-axis measurement plane is the plane containing the major axis. The minor-axis measurement plane is the plane containing the minor axis. The angle β is measured from the jet axis to the measurement location. Therefore, $\beta = 0°$ represents a point on the positive x-axis in the direction of the flow.

As described in McLaughlin, Barron & Vaddempudi (1992), the facility has been modified to mix helium with the main jet air flow. The jet then has a reduced density and higher acoustic speed (and jet velocity) compared to an unheated air jet. As a result, the helium/air mixture jet more closely simulates a heated jet by having a jet-to-ambient environment density ratio and jet velocity similar to an actual heated jet. By knowing the total pressures of air flow alone, the helium flow alone, and the total pressure of the combined helium/air flow, it is possible to calculate the helium

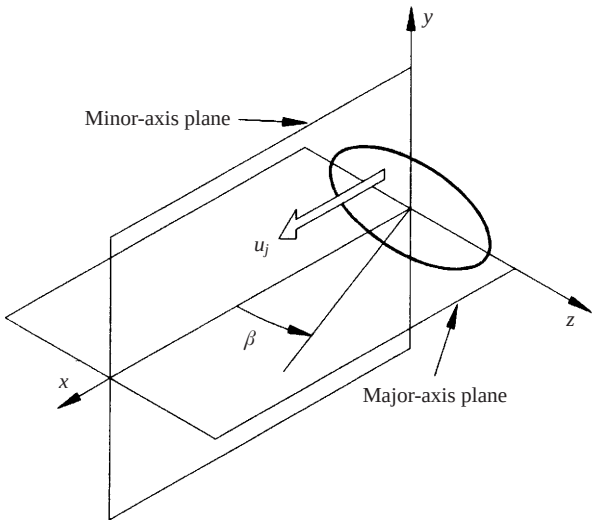

FIGURE 3. Measurement coordinate system and nomenclature.

Nozzle shape	M_j	D_{eq} (cm)	Helium concentration (by mass)(%)	T_j/T_a^*	u_j ($m\,s^{-1}$)	P_0 (torr)	P_j (torr)	Characteristic frequency, $f_c = u_j/D_{eq}$(Hz)	Reynolds number
Elliptic	1.48	1.38	0	0.69	425	101	28	30 800	27 000
Circular	1.6	1.00	0	0.66	445	160	37	44 500	27 000
Elliptic	1.5	1.38	26	1.2	690	185	47	50 000	27 000
Circular	1.61	1.00	23	1.1	690	240	51	69 000	27 000

TABLE 1. Experimental conditions.

concentration in the jet flow. Gas properties such as molecular weight and viscosity can then also be calculated. For the purposes of this work, the helium jet simulates a heated jet with $T_j/T_a^* = 1.2$ (the $*$ denotes a simulated temperature ratio). That means that the helium jet has the same jet acoustic speed and flow velocity as an actual heated jet with the same Mach number and jet-to-ambient temperature ratio (T_j/T_a) of 1.2. Because of the different ratio of specific heats of helium and air, the jet-to-ambient density ratio may not be an exact match in the simulation. A more through discussion of the helium delivery system is given in Kinzie & McLaughlin (1998).

Table 1 shows the operating conditions for the near-perfectly expanded jets reported in this work. Although both the circular and elliptic jet nozzles were designed to operate at the nominal Mach number 1.5, the circular nozzle ran at $M = 1.6$ for the present experiments. This is because this nozzle was originally designed to operate in the lower Reynolds number range ($Re < 10\,000$) with boundary layer corrections included in the nozzle contour design. Operations at higher Reynolds number produce a thinner boundary layer with more nozzle expansion to the higher Mach number. When operating the helium/air mixture jets, the helium concentration is set such that both jets have the same exit velocity, within experimental uncertainty. Throughout this paper, the temperature ratio for all air jets will be nominally referred to as

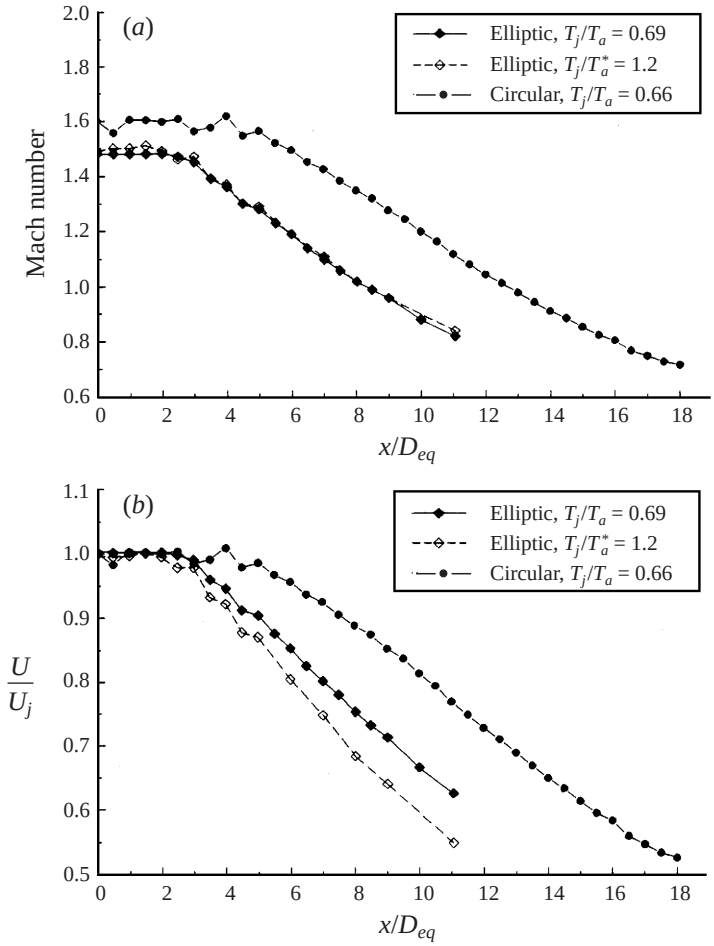

FIGURE 4. Centreline Pitot pressure measurements of natural jet: (*a*) Mach number distribution; (*b*) velocity distribution.

$T_j/T_a = 0.69$ and all helium/air mixture jet cases will be referred to nominally as $T_j/T_a^* = 1.2$. In addition, the 0% helium concentration cases will be referred to as pure air jets while the helium/air mixture jets are referred to as helium/air jets or simply helium jets.

3. Mean flow field measurements

3.1. *Centreline Mach number and velocity distributions – pure air jets*

Since the radiated noise is such a strong function of jet velocity, the axial centreline velocity distribution can give a rough indication of the axial region over which large amounts of noise are likely to be produced. The Mach wave emission process is only present in regions of the jet where the large-scale turbulence components have supersonic phase velocities (with respect to the ambient medium). Figure 4 shows the centreline Mach number and velocity distributions for the elliptic and circular jets. The pure air jet and the helium/air elliptic jet are all shown on the same plots. The axial distance is normalized by the jet equivalent diameter. Note that the round jet,

with its exit Mach number of 1.6 as discussed earlier, contains a small shock cell structure due to the slight imperfection associated with the boundary layer correction being made at a Reynolds number lower than the one used in the present experiments. The elliptic jet has a shorter potential core length than the circular jet. This shortening of the potential core agrees with the measurements of Seiner *et al.* (1992) in high Reynolds number non-circular jets.

The shortening of the potential core from the elliptic nozzle indicates that if both jets had the same exit area producing the same thrust, the circular jet would have a potential core longer than the elliptic jet. As a result, the round jet would have a larger high-velocity noise-producing region than the elliptic jet. Therefore, the axial extent of supersonically convecting turbulence capable of Mach wave emission in the elliptic jet should be reduced relative to a round nozzle.

3.2. *Centreline Mach number and velocity distributions – helium air jets*

The centreline Mach number and velocity distributions from the pure air elliptic jet are also compared to those of the helium/air mixture jet ($T_j/T_a^* = 1.2$) in figure 4. At the jet exit and in the potential core region, the Mach number of the helium elliptic jet is slightly higher than that of the pure air jet. This is due to the increase in the ratio of specific heats of the helium and the resulting minor change in the area ratio/Mach number relationship. After the potential core region, however, the Mach number and decay rate from both jets are virtually identical. However, the velocity data of the helium jet show an increased decay rate compared to the air jet with a very slight decrease in potential core length. According to the work of Lau (1981) and Seiner (1992) on axisymmetric jets, the potential core region generally contracts as the jet is heated accompanied by a corresponding faster decay of the centreline velocity. For a Mach number of 1.4, Lau shows a decrease in potential core length from approximately 6 to 4.5 diameters as the jet temperature is increased from isothermal to $T_j/T_a = 2.32$. Therefore, the data of figure 4 agree with the trends demonstrated in the previous research on actual heated jets.

3.3. *Velocity profiles*

Figure 5(*a–h*) shows velocity profiles as a function of the radial coordinate for the pure air elliptic jet at a Reynolds number of 27 000. These measurements were made with a five-probe Pitot rake and are normalized by the jet exit velocity. The centreline velocity for both axes does not begin to decay until an axial location of nearly $x/D_{eq} = 3$. At the end of the potential core, the minor-axis profile takes on a Gaussian-type distribution across the jet, while the major axis maintains a region of uniform velocity up to an axial distance beyond $x/D_{eq} = 5$. This results in the jet having a 'wedge-like' shape between the axial locations of $x/D_{eq} = 3$ to just after $x/D_{eq} = 5$. By $x/D_{eq} = 8$, the major axis also displays a Gaussian-like shape across the jet and the jet has become nearly axisymmetric. By $x/D_{eq} = 12$, profiles on both the major and minor axes are practically identical, indicating that the jet has developed an axisymmetric shape. This axisymmetry extends through the remaining measurement range to $x/D_{eq} = 17$.

It is interesting to note that up to the measurement range of $x/D_{eq} = 17$, there is no evidence of axis switching. This phenomenon is common on low-speed elliptic jets and in underexpanded elliptic jets. Hussain & Husain (1989), Zaman (1995), Schadow *et al.* (1989), and others have documented axis switching in elliptic jets in both the low-speed and underexpanded case. However, measurements by Seiner *et al.* (1992)

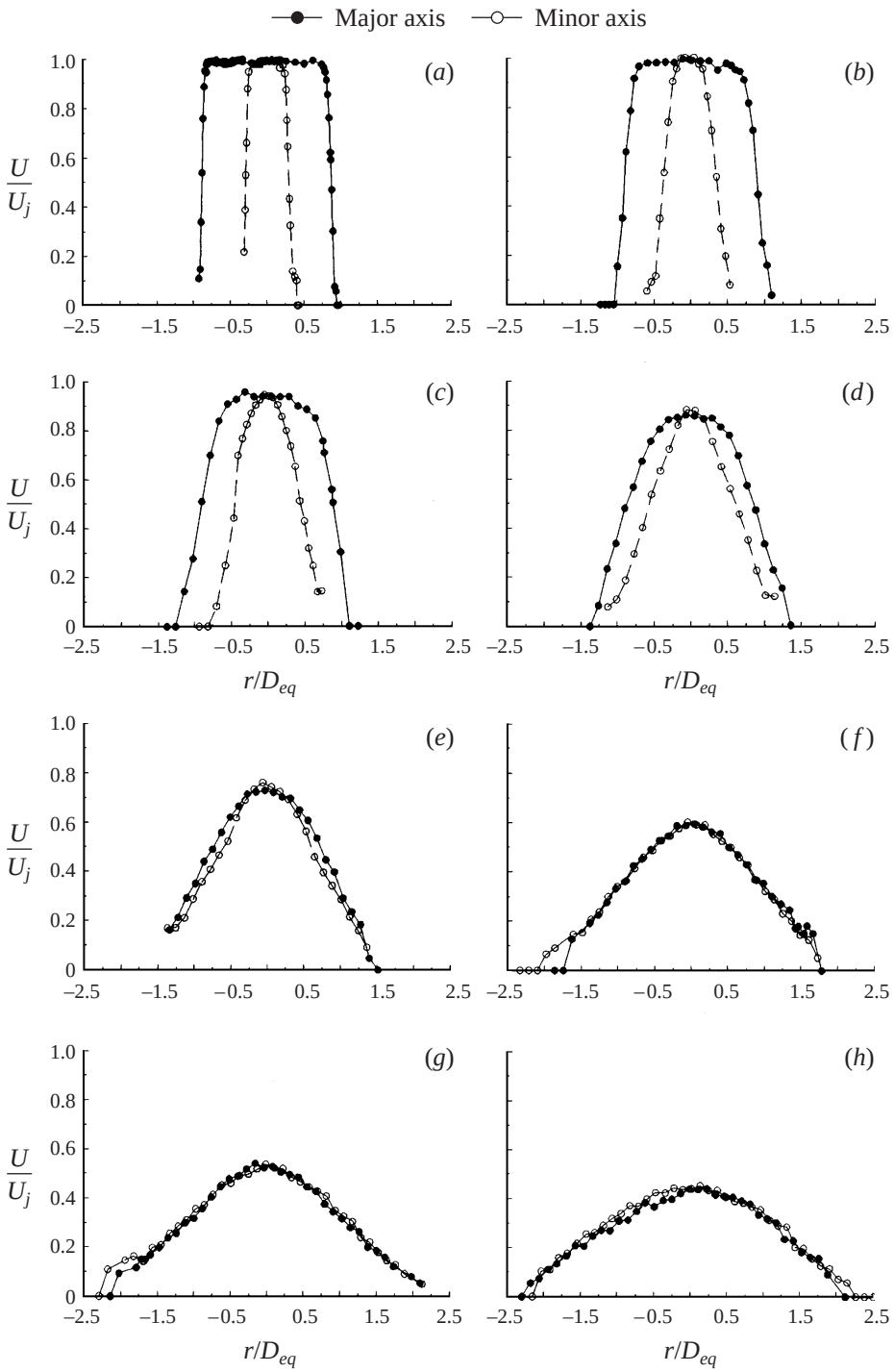

FIGURE 5. Velocity profiles for natural pure air elliptic jet, $T_j/T_a = 0.69$. (*a*) $x/D_{eq} = 1$, (*b*) $x/D_{eq} = 2$ (*c*) $x/D_{eq} = 3$, (*d*) $x/D_{eq} = 5$, (*e*) $x/D_{eq} = 8$, (*f*) $x/D_{eq} = 12$, (*g*) $x/D_{eq} = 14$, (*h*) $x/D_{eq} = 17$.

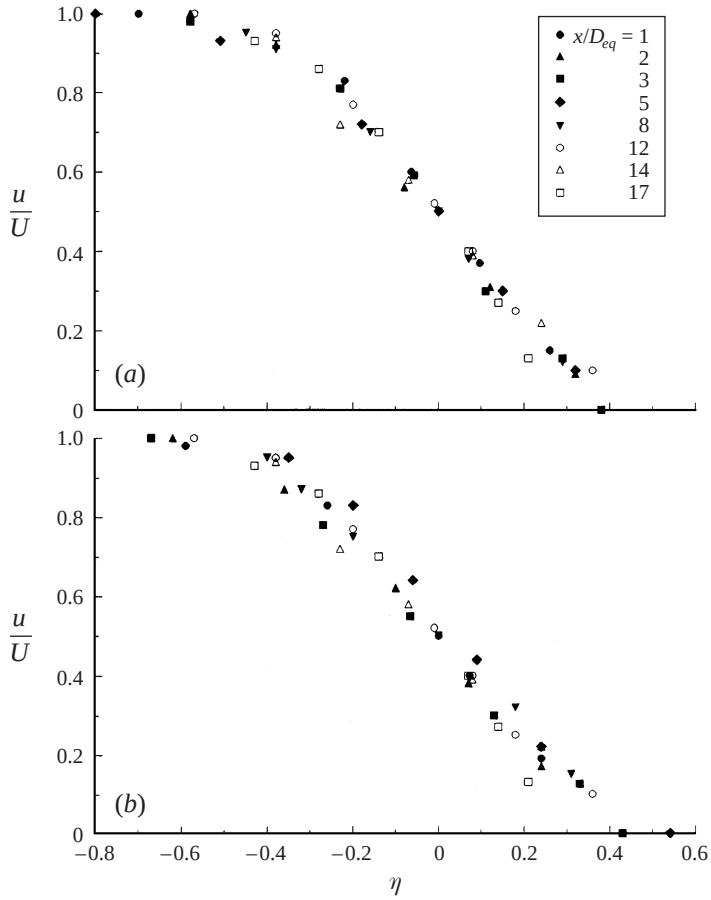

FIGURE 6. Normalized velocity profiles of the natural pure air elliptic jet, $T_j/T_a = 0.69$: (*a*) major axis, (*b*) minor axis.

also show no evidence of axis switching in a perfectly expanded Mach 2, $AR = 3:1$ elliptic jet to an axial distance of $x/D_{eq} = 30$.

3.4. *Normalized velocity profiles and vorticity thickness*

In order to develop a better understanding of the elliptic jet mean flow, the velocity profiles of figure 5 were normalized in the manner of Troutt & McLaughlin (1982). In figure 6, the local velocity is normalized by the jet velocity on the centreline at the axial measurement location. The radial distance, η, from the jet centreline is defined as

$$\eta = \frac{(y - y_{0.5})}{\delta},$$

where $y_{0.5}$ is the distance from the jet centreline to the radial location at which the velocity is half that on the centreline and δ is the jet shear layer thickness between 0.99 and 0.01 times the centreline velocity. This type of normalization has been shown by Troutt & McLaughlin (1982), Lau (1981), and others to collapse the velocity profiles of axisymmetric jets over a wide range onto a single universal curve.

Figure 6 shows the normalized velocity profiles for both the major and minor axes

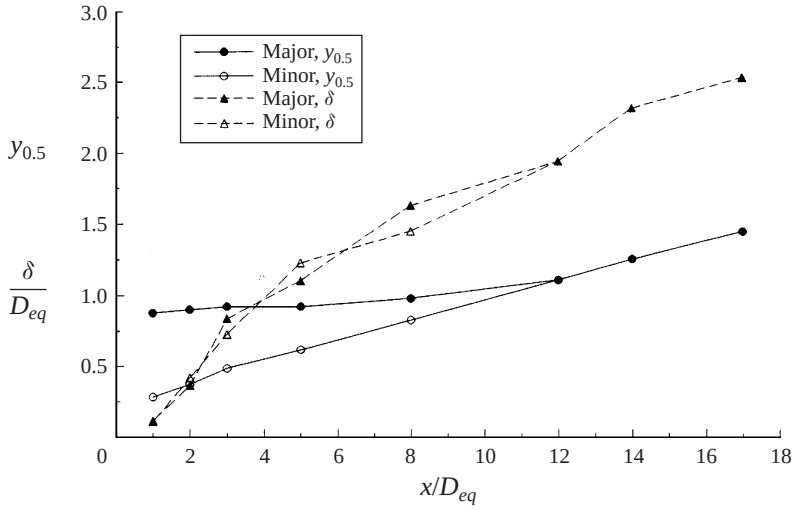

FIGURE 7. Thickness parameters used to normalize the jet velocity profiles of figure 6, $T_j/T_a = 0.69$.

of the pure air elliptic jet. Despite the asymmetry, the jet does have an element of self-similarity throughout the measurement range. The major axis fits the universal curve better than the minor axis.

Figure 7 shows the thickness parameters used to normalize the data of figure 6. The growth rate on the minor axis is higher than that on the major axis as defined by the half-velocity points. However, the shear layer thickness (δ) growth rates defined by the 0.99 and 0.01 velocity points are approximately equal on both axes. When discussing the spread rate of asymmetric jets, it is important to know exactly how the spread rate is defined.

4. Fluctuating flow-field measurements

4.1. *Hot-wire fluctuation amplitudes*

Figure 8(*a–d*) shows hot-wire spectra measured in the shear layer of the pure air elliptic jet at axial locations of $x/D_{eq} = 2, 3, 5$, and 7. For these measurements and all other similar hot-wire fluctuation measurements, the hot wire is placed at the approximate location of maximum r.m.s. amplitude. This is close to the jet lipline throughout the potential core region and then moves to the jet centreline downstream of the potential core. Also, unless stated otherwise, the orientation of the hot wire is perpendicular to the measurement plane in order to capture flow fluctuations parallel to the measurement plane. The amplitudes are normalized by the maximum mean-squared fluctuation level over all measurement locations. Therefore, the value of the ordinate of figure 8 is defined as

$$(\rho u)^* = \left\{ \frac{(\rho u)'}{(\rho u)'_{max}} \right\}^2 / \text{Hz}.$$

Early fluctuations in the minor-axis plane are characterized by peaks that appear and disappear in the spectra. The Strouhal number scale in figure 8 is calculated by normalizing the measured frequency by the characteristic frequency in table 1. The characteristic frequency, f_c, is equal to u_j/D_{eq}. By $x/D_{eq} = 3.0$, energy around

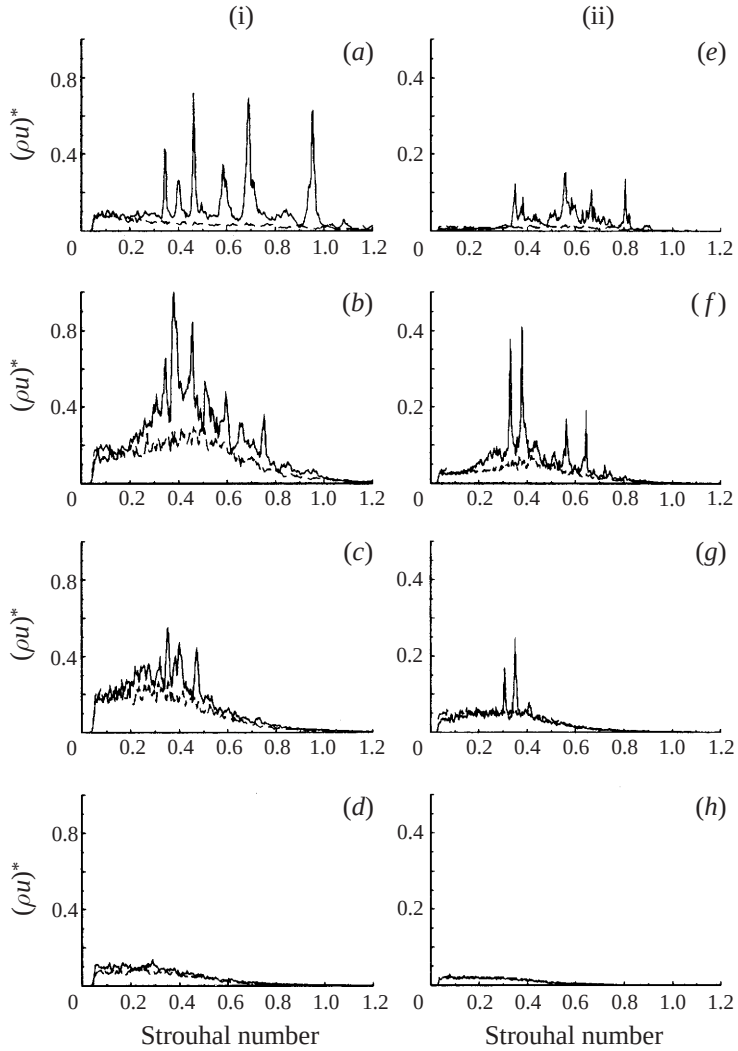

FIGURE 8. Hot-wire fluctuation measurements in the natural jet: ------, major axis; ———, minor axis. (i) $T_j/T_a = 0.69$, (ii) $T_j/T_a^* = 1.2$: (a, e) $x/D_{eq} = 2$, (b, f) $x/D_{eq} = 3$, (c, g) $x/D_{eq} = 5$, (d, h) $x/D_{eq} = 7$.

$St = 0.4$ shows the highest amplitude. These components grow and continue to have the highest amplitude to a location of $x/D_{eq} = 5.0$ where the highest levels begin shifting to lower frequencies. Morris & Bhat (1995) predict the $St = 0.4$ component to be close to the instability wave with the highest growth rate in a $M = 1.5$, $AR = 3$ elliptic jet.

Rather than showing sharp peaks as for the minor axis, the major-axis plane spectra show a much more broadband frequency content. In fact, the $St = 0.4$ component prevalent for the minor axis hardly shows any increase as the probe is traversed downstream. The levels of the individual frequency components are also generally lower in the major-axis plane than in the minor-axis plane. As will be shown shortly, this leads to lower overall fluctuation levels in the major-axis plane compared to the minor-axis plane.

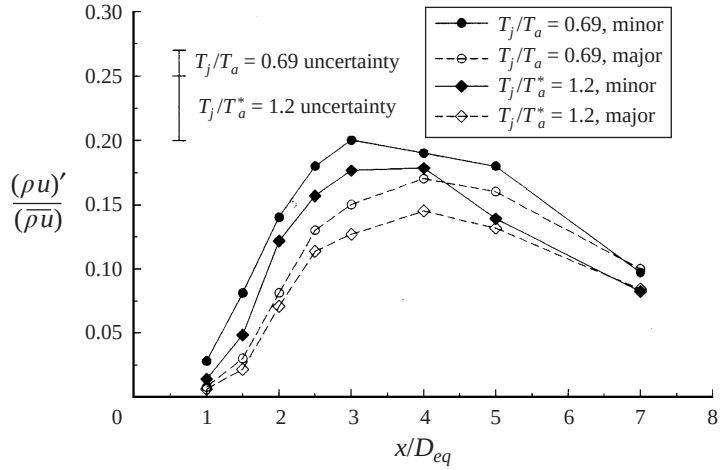

FIGURE 9. Overall mass-velocity fluctuation levels in natural elliptic jet as a function of axial distance from nozzle.

Figure 8(*e–h*) shows hot-wire spectra measured in the minor- and major-axis planes for the helium/air elliptic jet. In general, the spectra show the same trends as the air jet. The minor-axis plane shows narrow peaks throughout its development with the peak level located around $St = 0.38$. As with the air jet, the major-axis plane spectra tend to be flatter and of lower level than the minor-axis plane. Note that the characteristic frequency of the helium/air jet is considerably higher than for the air jet and that all dimensional frequencies of the simulated hot jet are similarly much higher than for the pure air jet.

The maximum mass-velocity fluctuation levels for the unexcited elliptic jet as a function of downstream distance are shown in figure 9. As implied by the individual spectra, the overall levels measured in the minor-axis plane are higher than those measured in the major-axis plane. The minor-axis plane shows higher fluctuation levels throughout the potential core region and then begins to approach the major-axis fluctuation levels further downstream. Both the pure air and helium/air jets show similar trends.

4.2. *Instability mode growth rates*

Tam & Morris (1980) showed that the radiated noise from a compressible mixing layer is strongly dependent on the growth and decay of individual frequency components in the shear layer. The frequency components with the highest axial growth rates, or most unstable components, are normally the ones that radiate the most noise to the far field. Morris & Bhat (1992, 1993) predict the flapping mode to have a higher growth rate than the varicose mode in a Mach 1.5, $AR = 3$ elliptic jet. Therefore, they also predict the flapping mode to radiate more strongly to the far field.

By exciting the jet in either a varicose mode or flapping mode and measuring the fluctuation amplitude as a function of axial distance, it is possible to determine the relative axial growth rate of each mode at a specific frequency. Figure 10 shows the fluctuation levels as a function of downstream distance for the pure air and helium/air mixture elliptic jets excited at a Strouhal number of 0.4. The slope of the curves give an indication of the growth rate of each mode. The initial exponential growth region noted by Troutt & McLaughlin (1982) in a Mach 2 round jet is less apparent in the

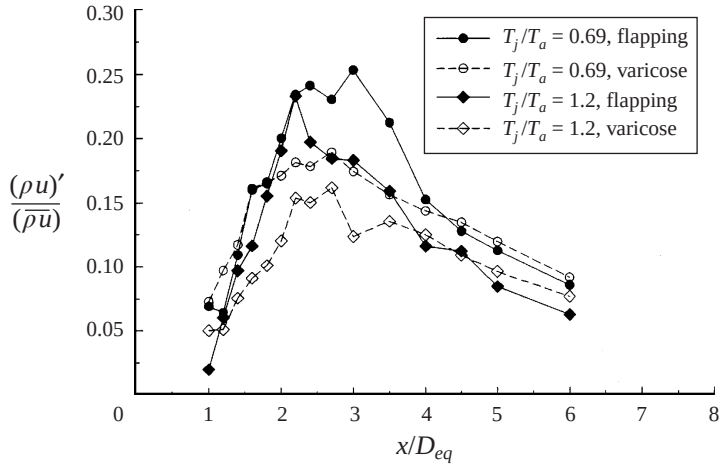

FIGURE 10. Fluctuation amplitudes in elliptic jet excited at $St = 0.4$ showing the growth rate of individual modes.

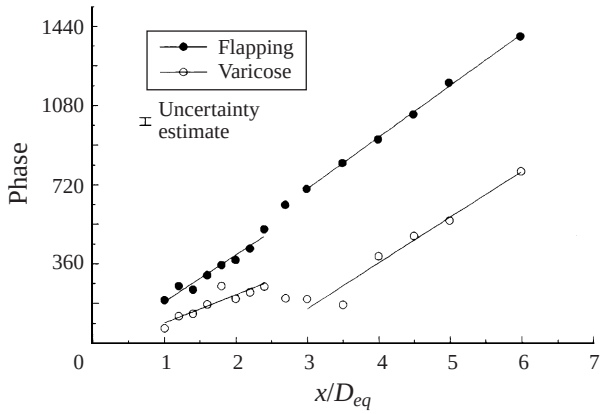

FIGURE 11. Axial phase distribution for the pure air elliptic jet excited at $St = 0.4$, $T_j/T_a = 0.69$.

present measurements. The flapping mode does show a higher growth rate than the varicose mode for both jet conditions.

From these data, it might be expected that the flapping mode will radiate more noise than the varicose mode for both the air and helium/air jets. However, it will be demonstrated that the phase speed of each mode plays a significant role in how efficiently each mode radiates to the far field. Additionally, since the flapping mode radiates primarily in the minor-axis plane, one might expect to measure higher noise levels in that plane due to the flapping. This is in fact the case as will be shown by the acoustic measurements.

4.3. *Axial phase speed*

Since the phase velocity of the spectral components of the large-scale structures is such an important parameter relative to Mach wave emission, an effort has been made to measure the convection speed of the structures. Figure 11 shows the axial phase distribution for the pure air elliptic jet excited at a Strouhal number of 0.4 obtained by cross-correlation of the excitation signal with the hot-wire signal. For

the regions where the phase distribution is a linear function of axial distance, the slope of the line can be used to calculate the wavelength of the instability wave. The wavelength, λ, is equal to $360°/m$ where m is the slope of the line as shown in figure 11. Since the excitation frequency is known, the convection velocity of the wave can be calculated ($U_c = f\lambda$). Note that convection velocity is inversely proportional to the slope of the phase plot.

It is apparent from the major dislocation of phase at the end of the potential core region (and perhaps earlier) in figure 11 that the convection velocity of the structures changes at this location in the jet. In the potential core region, the data of figure 11 show the flapping mode to have a phase velocity relative to the jet exit velocity of 0.75. The irregularity in the phase distribution in the potential core region of the varicose data make an estimation of the phase velocity with reasonable confidence impossible. A rationale for these irregularities is discussed in the next section. In the meantime phase data with these types of uncertainties are not presented in the present discussion. Reliable data show that downstream of the potential core, the varicose mode has a phase velocity of 0.77 times the jet exit velocity and the flapping mode has a phase velocity of 0.68 times the jet exit velocity.

Measurements like those shown in figure 11 were made over a range of Strouhal numbers in order to obtain a better understanding of the jet instability waves. In the potential core region, it was not possible to obtain reliable measurements for a wide Strouhal number range. As a result, only measurements in the region just downstream of the potential core are reported here.

Figure 12(a) shows the phase velocity of the instability waves as a function of Strouhal number for the pure air elliptic jet. In general, the varicose mode has a higher velocity than the flapping mode and the phase velocity increases with increasing Strouhal number, except at the highest frequencies. The horizontal line represents the phase velocity equivalent to the ambient speed of sound normalized by the jet exit velocity. Therefore, structures with phase velocities above this value will radiate noise through Mach wave emission. Except for the varicose mode at $St = 0.44$, no Strouhal number component exceeds this value for the air jet case.

Figure 12(b) shows the same measurements for the helium/air elliptic jet. Again, the varicose mode shows a higher velocity compared to the flapping mode. The stability analysis of Morris & Bhat (1993) also predicts the varicose mode to have a higher phase velocity than the flapping mode for both the cold and heated jet conditions. They also predict the phase velocity of both modes relative to the jet exit velocity to decrease as the jet is heated. In general, the present measurements also show these trends, although the varicose mode does show a slight velocity increase for some frequencies when helium is added. Therefore, the present results agree with the predictions of Morris & Bhat (1993) that jet heating causes the instability wave phase velocity to increase with respect to the ambient sound speed, but decrease with respect the jet exit velocity.

Note that for the helium/air case, the phase speed of the varicose mode exceeds the ambient speed of sound over nearly the entire Strouhal number range while the flapping mode is close to, but just below, the sonic value. Tam & Morris (1980) showed that because of the contribution from the strong growth, near-sonic instability waves can have supersonic wavenumber components which will radiate to the far field. Evidence of the stronger coupling of the hydrodynamic pressure field to the acoustic field at the higher jet velocity will be seen in the modal decomposition measurements of the helium/air elliptic jet. Also, far-field acoustic data to be presented later show evidence that this increase in instability wave phase velocity compared to the ambient

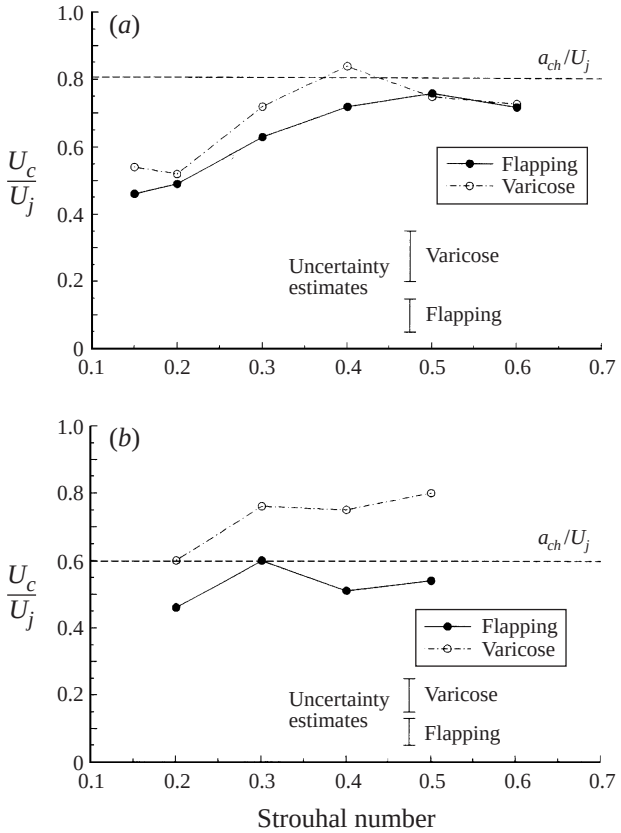

FIGURE 12. Phase speed as a function of Strouhal number in an artificially excited elliptic jet (downstream of the potential core): (*a*) pure air jet, $T_j/T_a = 0.69$, (*b*) helium jet, $T_j/T_a^* = 1.2$.

sound speed corresponds to an increase in acoustic radiation consistent with Mach wave emission.

4.4. *Radial hot-wire measurements*

As discussed earlier, it is very difficult to obtain consistent phase measurements in the potential core region of the jet such that an instability wave convection speed can be determined reliably. This section addresses this issue and attempts to provide an explanation for the additional complications associated with the measurement of the relative phase distributions in the jet shear layer. Figure 13 shows the relative phase between the hot-wire signal and the glow excitation signal as the hot wire is traversed radially across the pure air elliptic jet shear layer with the axial measurement location held constant. The axial location is $x/D_{eq} = 1.8$, about midway through the potential core region and the jet is excited by the flapping mode at $St = 0.4$. The r.m.s. fluctuation amplitude for each position is also shown. There is approximately a 360° phase shift across the shear layer and two peaks in the r.m.s. fluctuation distribution. For most of the hot-wire measurements discussed until now, the hot wire has been located at the point of maximum r.m.s. fluctuations seen in figure 13.

It is seen from the phase distribution that there is a relatively narrow plateau of constant phase both on the inner and outer edges of the shear layer. Between these

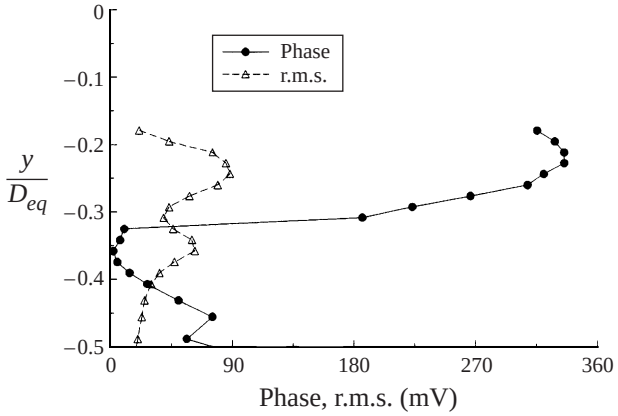

FIGURE 13. Phase distribution across the artificially excited pure air elliptic jet shear layer at $x/D_{eq} = 1.8$, flapping mode, $T_j/T_a = 0.69$, $St = 0.4$.

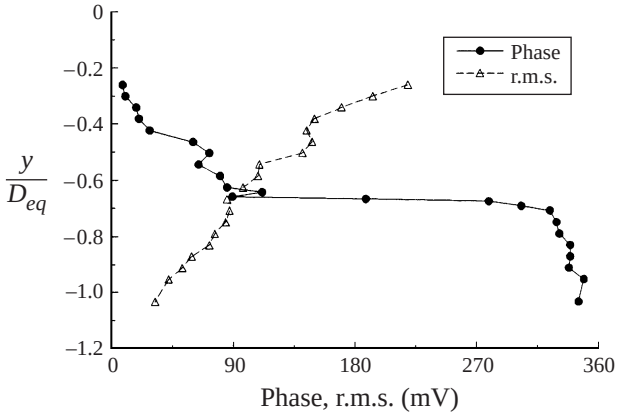

FIGURE 14. As figure 13 but at $x/D_{eq} = 3.5$.

plateaux is a region where the phase changes rapidly across the shear layer. The whole shear layer is located within the two r.m.s. humps with a thickness of approximately $0.2D_{eq}$. This is a thin region less than 3 mm thick. Therefore, it is not surprising that the measurement of consistent axial phase distributions is difficult when there is such a large phase change occurring over such a narrow measurement range. Moving the probe downstream can lead to irregular phase measurements, or phase 'dislocations' as referred to in § 4.3.

Figure 14 shows the radial phase measurements across the pure air elliptic jet shear layer excited at a Strouhal number of 0.4 at an axial location of $x/D_{eq} = 3.5$, just downstream of the end of the potential core. This time, there is approximately a 270° phase change across the shear layer. However, the shear layer is much thicker and therefore the change is more gradual. This type of phase distribution is more conducive to the estimation of axial phase velocity than those in the relatively thin shear layer surrounding the jet potential core.

The general trend of the present work, therefore, is that the phase distribution across the shear layer shows approximately a 360° change in the potential core region and then a somewhat lower phase change further downstream in the jet. However,

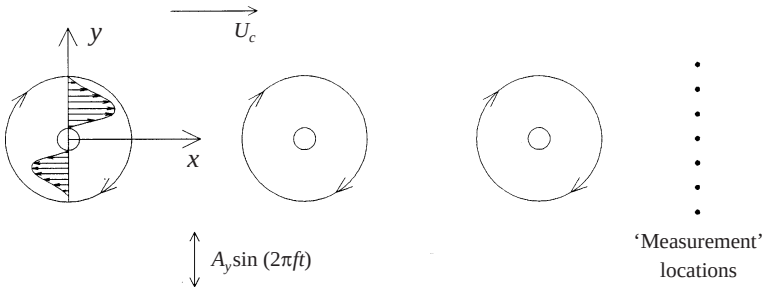

FIGURE 15. Schematic of vortex model.

there are some variances to this trend over the test matrix of the present work. A totally consistent and unifying description of the phase changes and conditions under which they are produced is not possible from the present data.

The radial phase distributions seen in figures 13 and 14 show similar trends to those predicted and measured in a low-speed planar shear layer by Gaster, Kit & Wygnanski (1985). At a moderate axial distance downstream, they show an approximately 270° phase shift across the mixing layer. Father downstream, their phase change is lower and is approximately 200° across the shear layer. As in the present work, they also show a double peak in their r.m.s. profiles at early axial locations. These similarities suggest that the dynamics of mixing in both high- and low-speed shear layers share some fundamental characteristics.

Flow visualization from both high- and low-speed mixing layers shows that shear layers are composed of vortical-like structures which grow in size as the layer develops (Martens, Kinzie & McLaughlin 1994; Winant & Browand 1974). In an effort to learn more about the basic structure of mixing layers, a qualitative analytical model has been developed based on the principle of travelling vortices. The present model assumes that the large-scale structures in a mixing layer can be simulated by vortices convecting downstream while at the same time oscillating in the transverse direction to simulate additional 'waviness' of the mixing layer. This is shown schematically in figure 15. The model is similar to one used by Winant & Browand (1974) to describe the velocity field in a train of vortices in advance of the vortex pairing process in a low-speed shear layer.

The velocity components of each vortex are written as

$$u = C_u\, y\mathrm{e}^{-R}, \quad v = -C_v\, x\mathrm{e}^{-R},$$

where u and v are the x- and y-components of velocity, respectively, and R is the distance from the centre of the vortex. C_u and C_v are constants assumed to be unity for this analysis. Note that there is a quiescent region of fluid near the centre of each vortex since the velocity approaches zero for small values of R. The u-component of velocity on the high-speed side of the simulated shear layer is also increased by approximately 20% over the u-component of velocity on the low-speed side to simulate a non-uniform mean velocity profile. In addition to a convection speed in the x-direction, a small oscillation in the y-direction is added to the vortex motion. The centre of the vortex therefore traces out a sinusoidal wave of specified amplitude and frequency. The model then simulates a train of vortices which convect in the x-direction while simultaneously oscillating in the y-direction. Cross-correlation of the calculated velocity at a specified location with the y-oscillation forcing function is then analogous to a cross-correlation of a hot-wire signal with an excitation signal artificially forcing the mixing layer of

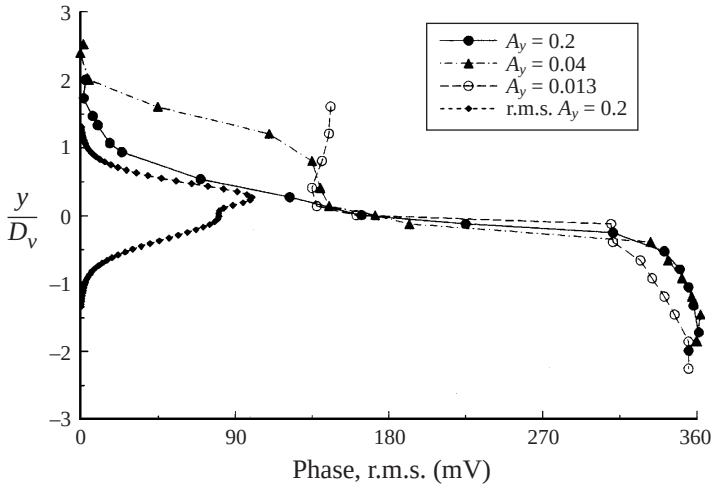

FIGURE 16. Predicted phase and r.m.s. distribution across the vortex row.

the jet. The relative phase and r.m.s. amplitude can then be calculated using the same methods as described for the supersonic jets of the present work.

Figure 16 shows the phase and r.m.s. amplitude distribution across the vortex train as the magnitude of the y-oscillation is changed from $A_y = 0.2$ to $A_y = 0.013$. The r.m.s. amplitude distribution is shown for the case where $A_y = 0.2$. The vertical position across the vortex train and the y-oscillation amplitude are normalized by the diameter of the vortex (D_v) where the velocity has decreased to 1% of its maximum value. For this example, vortices are spaced approximately $1.32D_v$ apart and they convect downstream with a Strouhal number of approximately 0.8. Since there are no compressibility or viscous effects included, this simple numerical model is relatively insensitive to size, spacing, and frequency of the vortices. For a given frequency, the oscillation amplitude is the main driver of the measured phase distribution across the vortex train. Therefore, the intent of this analysis is to examine the qualitative behaviour of the mixing layer as the vortices convect downstream and it is not intended to model any specific flow conditions

There is approximately a 360° phase change across the vortex row when the amplitude of vortex oscillation with respect to the vortex size is high ($A_y = 0.2$). This is the same phase change observed in the early stages of the mixing layers investigated in the present work. At the lowest amplitude of vortex oscillation ($A_y = 0.013$), there is only a 180° phase change across the vortex row. The intermediate oscillation amplitude ($A_y = 0.04$) shows an irregular distribution as it makes a 360° phase change across the vortex train.

This simple model offers some qualitative insight into the radial phase distribution across a shear layer where a combination of convecting vortical lumps and smoother wave-like structures is expected. Early in the actual shear layer development, it is hypothesized that the mixing layer can be modelled by vortices that oscillate with a relatively high amplitude with respect to their small size. As seen by the model prediction, this produces a near 360° phase change across layer and is in agreement with the measurements of the present work at axial locations close to the initial formation of the jet shear layer. As the vortices grow and the shear layer thickens, the relative amplitude of their excursion from some mean cross-stream location is lower compared to the vortex size. For these conditions, the model then predicts the

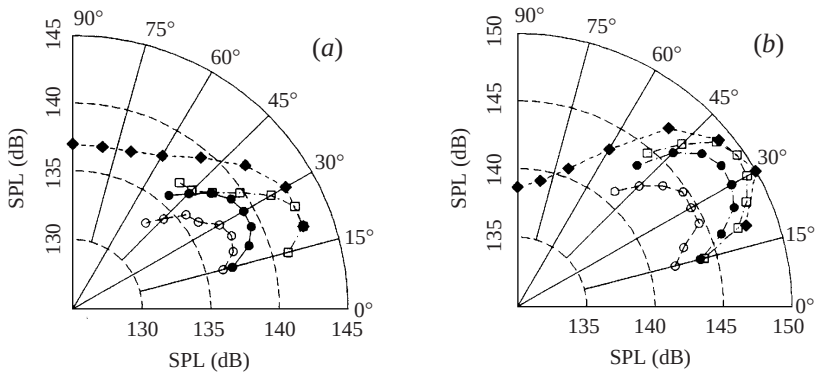

FIGURE 17. SPL directivity arcs; natural jets, $R/D_{eq} = 25$: •, elliptic, minor axis; ○, elliptic, major axis; □, axisymmetric jet; ◆, M*S prediction. (*a*) $T_j/T_a = 0.69$, (*b*) $T_j/T_a^* = 1.2$.

phase difference across the layer to be approximately 180°. The present experiments show approximately a 270° phase shift across the jet shear layer and Gaster *et al.* (1985) show a near 200° phase change across the layer at the farthest downstream measurement location. These experimental observations are consistent with the trend of the analytical model which predicts the phase difference across the vortex row to decrease from 360° to 180° as the size of the vortices grows in comparison to their cross-stream oscillation amplitude.

In addition to a reasonably good prediction of the phase distribution across the shear layer, the model also qualitatively predicts the double peak in the r.m.s. distribution. As in the present work, this double peak is often observed in the r.m.s. fluctuation distribution across both high- and low-speed free shear layers (see Winant & Browand 1974; Demetriades & Brower 1982; Oster & Wygnanski 1982; Martens 1995). From velocity measurements in a low-speed shear layer, Oster & Wygnanski (1982) conclude that the double peak arises from the passage of 'vortex lumps' past a measurement plane with high-velocity regions surrounding a quiescent core region. Their conclusion is supported by the present model. The higher peak is always seen to be next to the high-speed side of the shear layer. The higher fluctuation level next to the high-speed side of the shear layer apparently arises from the asymmetry of the vortex which is skewed toward the high-speed side.

5. Acoustic measurements

This section presents a discussion of the acoustic properties measured in the model jets. Up to this point, the results and discussion have focused on the aerodynamic characteristics of the jets. Because the jet flow field has such a direct bearing on how the noise is produced and radiated in supersonic jets, it has been important to establish a firm understanding of the mean and fluctuating flow-field properties. Now, as data are presented from microphones in the jet acoustic field, the previously discussed flow data are available to aid in the interpretation of the acoustic results.

5.1. *Sound pressure level (SPL) directivity*

SPL directivity distributions along arcs of $R/D_{eq} = 25$, centred at the nozzle exits, are shown in figure 17(*a*) for the pure air elliptic and circular jets. This radius ranges from 3 to 30 times the acoustic wavelength over the Strouhal number range of 0.1 to 1.0, which makes these measurements representative of the acoustic far field. Because

of the limited size of the anechoic chamber, full arcs at $R/D_{eq} = 25$ are not possible. The major noise radiation direction is accessible since the peak noise directions are between $\beta = 25^\circ$ and 30° for all cases. For shock-containing jets, measurements are also required in the forward quadrant to properly characterize the dominant acoustic field. The minor-axis plane of the elliptic jet is louder than the major-axis plane. Referring to the hot-wire data, this relative noise difference results from the higher fluctuation levels in the minor-axis plane compared to the major-axis plane and the higher growth rate of the flapping mode, which will radiate predominately in the minor-axis plane. The non-circular jet also emits less total noise than the round jet.

Figure 17(*b*) shows the same measurements for the helium/air jets. It is clear that the helium jets radiate more noise at a higher angle to the jet axis compared to the pure air jets. The peak noise angles for the helium jet cases have increased to between 30° and 35°. The major-axis plane of the elliptic jet is 4–5 dB quieter than the circular jet. Also, the relative difference between the major- and minor-axis planes of the elliptic jet has increased. A similar phenomenon was also observed by Seiner *et al.* (1992) in measurements of a heated Mach 1.5 elliptic jet. The increased relative noise reduction at higher velocities is attributed to the ability of the non-circular jets to mix faster compared to the axisymmetric jet. As a result, Mach wave emission, which becomes more powerful as the jet velocity increases, is suppressed more by the increased mixing characteristics of the non-circular jet at the higher jet velocity compared to the lower velocity conditions. This characteristic could be exploited in an aircraft engine design by directing the quieter plane toward a direction creating less impact on community noise. Complete near-field SPL contours were also measured for the pure air and helium/air elliptic jets. These data are presented and discussed in Kinzie (1995) and are consistent with the directivity data presented in figure 17.

Also shown in figure 17 are predictions for a circular jet using the M*S methodology described in Gliebe, Motsinger & Sieckman (1978). M*S is a well established semi-empirical prediction tool used in industry for the prediction of noise radiated from high-speed heated jets. In order to better compare the trends of the present experimental data with the predictions, the peak SPL value for the predictions of the unheated jet was matched to the peak SPL value of the pure air experimental jet and that difference was added to *all* of the predicted values. Therefore, a constant value of 3.3 dB was added to the M*S predictions for both the unheated and heated jet cases. With this adjustment to the predictions, the comparison between the measured and predicted directivities is quite good. In particular, the changes in overall SPL and directivity as the simulated jet temperature increases agree well with the actual hot jet prediction. This comparison is evidence of the ability to accurately simulate the noise generation characteristics of actual heated jets using the helium/air simulation.

5.2. *Acoustic spectra*

Acoustic spectra for $\beta = 25^\circ$ and $\beta = 40^\circ$ measured at $R/D_{eq} = 25$ corresponding to the overall SPL measurements are shown in figure 18 for the pure air jet. At $\beta = 25^\circ$, the peak noise levels are around $St = 0.25$ in both axis planes. For Strouhal numbers less than approximately 0.4, the levels in both planes are nearly equal. The increased overall noise levels measured in the minor-axis plane are due to spectral components above $St = 0.4$.

It is interesting to note that the peak acoustic frequencies for the air jet case tend to be lower than those of the peak fluid dynamic fluctuations measured by the hot wires (see figure 8). The measurements of Troutt & McLaughlin (1982) and Morrison & McLaughlin (1979) showed hot-wire spectra and acoustic spectra to

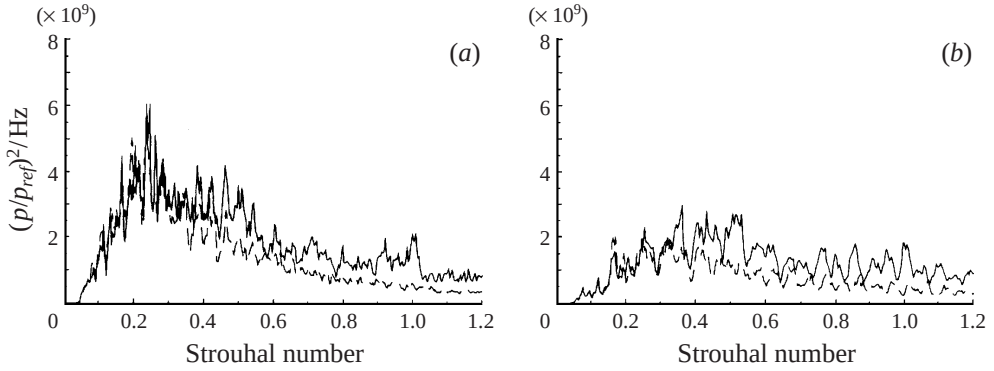

FIGURE 18. Far-field acoustic spectra of natural pure air elliptic jet, $R/D_{eq} = 25$, $T_j/T_a = 0.69$: ------, major axis; ——, minor axis. (*a*) $\beta = 25°$, (*b*) $\beta = 40°$.

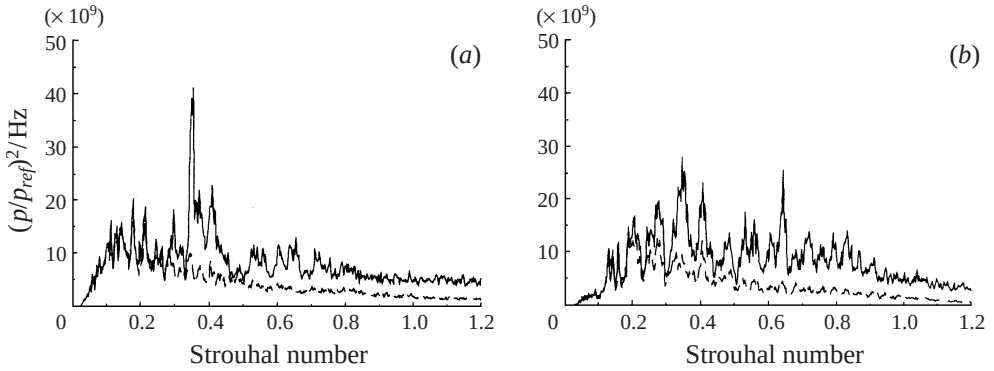

FIGURE 19. As figure 18 but for a natural helium elliptic jet, $T_j/T_a^* = 1.2$.

have similar spectral content for reduced Reynolds number Mach 1.5 and Mach 2.0 axisymmetric jets. However, as in the present work, Stromberg, McLaughlin & Troutt (1980) observed the radiated acoustic spectra to have lower frequency content than the hot-wire spectra in a Mach 0.9 low Reynolds number round jet. This phenomenon will be discussed again after the helium jet spectra are presented.

Figure 19 shows the acoustic spectra measured for the helium elliptic jet for locations corresponding to $\beta = 25°$ and $\beta = 40°$ at $R/D_{eq} = 25$. As in the pure air case, the major- and minor-axis planes show similar levels for the very low-frequency range. However, above a Strouhal number of approximately 0.3, the minor-axis plane shows significantly higher fluctuation levels compared to those in the major-axis plane. This accounts for the larger relative noise difference between the two planes observed in the overall SPL distributions of the helium jet compared to the air jet.

The acoustic spectra on the minor-axis plane also are very similar to those measured by the hot wire in the jet shear layer (figure 8). Because of their increased phase velocity relative to the ambient environment for the helium jet case, it is believed that these Strouhal number components now radiate directly to the acoustic field. Tam, Chen & Seiner (1992) state that for the Mach wave emission process, the Strouhal number

of the peak radiated noise should be the same as the most amplified instability wave. The present work agrees with this theory for the helium/air case. Recall that the data of figure 9 show higher hot-wire fluctuation levels in the minor-axis plane and that the data of figure 10 show the flapping mode to have a higher growth rate than the varicose mode. Since the flapping mode will radiate more sound in the direction of the flapping motion, all of this evidence leads one to expect higher noise levels in the minor-axis plane (as seen in the SPL measurements and acoustic spectra). Also, the azimuthal modal decomposition to be presented shortly shows that the peak spectral components of figure 19 are composed mostly of the flapping mode.

The comparisons of the acoustic and flow spectra of the air and helium jets suggest that the pure air elliptic jet produces noise in a fashion more consistent with subsonic jets in terms of displaying a nonlinear relationship between the flow fluctuations and the radiated noise as measured by Stromberg, McLaughlin & Troutt (1980). This is in contrast to the helium jet case where there is a more direct correlation between the measured flow fluctuations and the acoustic field pressure fluctuations. The observations in the helium jet case are consistent with the concept of Mach wave radiation from high-speed jets (Morris & Tam 1979; Tam *et al.* 1992; Tam & Chen 1994).

The unheated Mach 1.5 measurements of Morrison & McLaughlin (1979) indicate that the round jets in this speed range are closely related to higher Mach number jets with regard to noise generation. The present work, however, suggests that the noise generation of the Mach 1.5 elliptic jet may have more in common with lower Mach number round jets. This may be attributed to the increased mixing of the elliptic jet compared to the axisymmetric jet. Seiner (1992) showed that the normalized centreline velocity distribution from a Mach 1.52 elliptic jet was nearly identical to that from a Mach 0.86 round jet with regard to potential core length and decay rate. As a result, it is possible that the noise generation processes have similarities as well.

5.3. *Modal decomposition*

In order to determine the azimuthal behaviour of the large-scale turbulent fluctuations, a modal decomposition procedure similar to that performed by Troutt & McLaughlin (1982) and Hu & McLaughlin (1990) was developed for the elliptic jet. The previous authors were able to determine the modal content of supersonic jets by cross-correlating the signal from a fixed reference microphone in the acoustic field of the jet with the signal from a second microphone traversed around the azimuth of the jet. A Fourier decomposition performed on the data yielded the relative amplitude of each mode. A similar procedure is used in the present work using Mathieu functions as the basis for the Fourier decomposition in an elliptic cylindrical coordinate system. A detailed description of the technique is given in Kinzie & McLaughlin (1997).

Figure 20 shows modal decomposition results for the lowest two orders of the varicose and flapping modes for the unexcited pure air elliptic jet. The amplitudes have been normalized by the maximum value of the ce_0 mode. The jet is dominated by the even modes over all frequencies. Also, the higher frequencies are seen to be composed mostly of the higher-order varicose mode. There is a slight increase in the energy of the lowest-order flapping mode (se_1) between Strouhal numbers of 0.4 and 0.5. Baty, Seiner & Ponton (1990) used a similar technique to measure the azimuthal modes in an unheated Mach 1.5 elliptic jet with an aspect ratio of 2 and also found the jet to be composed primarily of the varicose mode.

Figure 21 shows the same measurements for the helium/air jet simulating a temperature ratio of $T_j/T_a^* = 1.2$. Now, in addition to the varicose modes, there is a

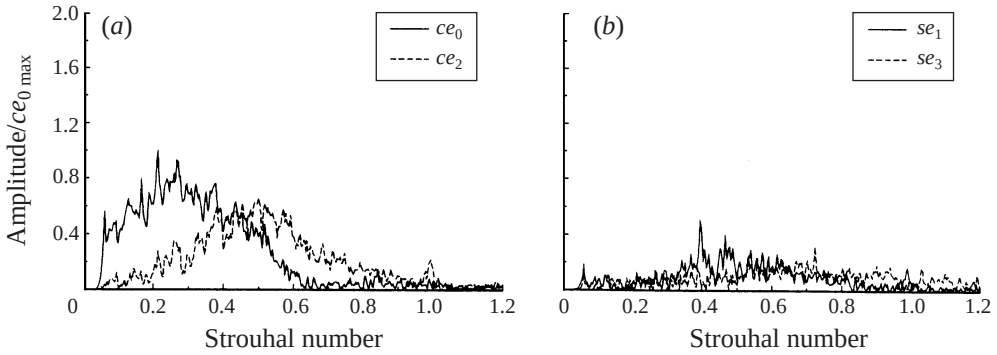

FIGURE 20. Modal content of natural pure air elliptic jet, $T_j/T_a = 0.69$. (*a*) Even modes, (*b*) odd modes.

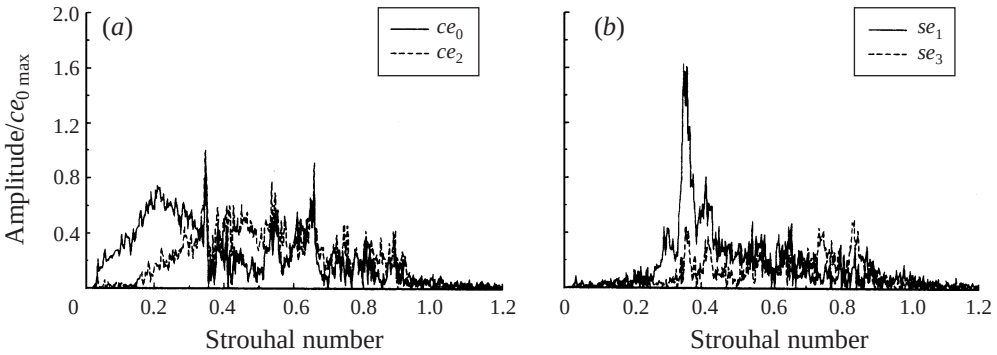

FIGURE 21. As figure 20 but for a natural helium mixture elliptic jet, $T_j/T_a^* = 1.2$.

significant increase in the flapping (se_1) mode compared to the pure air jet case, particularly in the midrange frequencies. Using an instability-wave-type theory, Tam & Chen (1994) also predict an increase in the number of azimuthal modes present in a circular jet as the jet temperature increases. The present measurements are consistent with that theory. The increased flapping mode in the jet acoustic field demonstrates a fundamental difference between the pure air and the helium jet that likely extends to the actual heated and unheated jet case.

Several interesting observations can now be made by comparing the far-field acoustic spectra shown in figures 18 and 19 and the modal content spectra shown in figures 20 and 21. For the pure air jet case, the peak noise frequency is close to a Strouhal number of 0.25 and the spectral shape is similar to that of the ce_0 mode shown in figure 20(*a*). However, for the helium mixture case, the peak frequency in the noise spectrum shifts to a higher value close to $St = 0.4$ and the far-field spectrum for the helium mixture case bears a strong resemblance to the modal decomposition spectrum for the flapping (se_1) mode (see figure 21*b*). It is interesting to note that the major-axis far-field acoustic spectra and the varicose modal spectra did not change significantly on going from the pure air jet case to the helium/air mixture case. Presumably it is predominantly the varicose mode that is radiating to the major-axis far field and this mode is not significantly affected by the simulated temperature increase of the jet. The flapping mode, on the other hand, radiates predominantly in the minor-axis direction and is strongly affected by the simulated jet heating. This

observation is in agreement with the predictions of Morris & Bhat (1993, 1995) for an elliptic jet with similar operating conditions.

Some caution should be exercised in the interpretation of the present modal decomposition measurements. The measurement locations were on a radius of approximately $r/D_{eq} = 4$ which is in the 'near' acoustic field clearly outside the hydrodynamic field. Thus, the measurements represent the modal content of the acoustic field and not necessarily the jet flow field itself. It is reasonable to conjecture, particularly for the lower-temperature relatively low supersonic jets, that the flapping mode may be more dominant in the jet flow field than the present measurements initially indicate. This would be the case in particular if the efficiency of the flapping motion in radiating to the far field is less than the varicose motion. Careful interpretation is of particular importance since the phase velocities of these instabilities for the Mach 1.5 cold jets are typically below the ambient sonic velocity whereas measurements show that for the helium/air mixture case, the phase velocities are close to or possibly even higher than the ambient sound speed. The instability wave phase speed plays a major role in the instability's acoustic radiation efficiency.

6. Conclusions

These data demonstrate beneficial properties of the elliptic jet with respect to increased mixing and noise reduction. The present work also provides a clearer understanding of the nature of non-circular jet noise and how it differs from sound generated by round jets.

The helium simulation of heated jets is able to successfully reproduce many of the aeroacoustic characteristics of actual heated jets. Strong evidence of Mach wave radiation is observed only when helium is added to the jet flow for these Mach 1.5 jets. Some of the observed changes for the simulated heated conditions are an increase in the phase velocity of the large-scale structures with respect to the ambient acoustic velocity, more noise produced in a more directional manner, peak instability frequencies radiating noise directly to the far field, and an increased amplitude of the flapping mode compared to the varicose mode. All of these qualities have either been measured in actual heated jets or agree with predicted trends caused by jet heating.

This study has further demonstrated the necessity of performing experiments or calculations recognizing the changes which take place as a jet is heated to realistic engine exhaust operating conditions. If the Mach wave emission noise source is not reproduced properly, it is possible to draw misleading conclusions while interpreting the data. The helium simulation of heated jets is relatively easy and provides a low-cost means to investigate these effects in small-scale supersonic jets.

This research project has been supported by NASA Langley Research Center through Grant NAG-1-1047, monitored by Dr J. M. Siener. The authors are also grateful to Dr P. J. Morris for his helpful discussions about this work.

REFERENCES

Baty, R. S., Seiner, J. M. & Ponton, M. K. 1990 Instability of a supersonic shock-free elliptic jet. *AIAA Paper* 90-3959.

Crow, S. C. & Champagne, F. H. 1971 Orderly structure in jet turbulence. *J. Fluid Mech.* **48**, 547–591.

Detmetriades, A. & Brower, T. L. 1982 Experimental study of transition in a compressible free shear layer. *AFOSR TR* 83-0144.

Ffowcs Williams, J. E. 1963 The noise of turbulence travelling at high speed. *Phil. Trans. R. Soc. Lond.* A **255**, 469–503.

Gaster, M., Kit, E. & Wygnanski, I. 1985 Large-scale structures in a forced turbulent mixing layer. *J. Fluid Mech.* **150**, 23–39.

Gliebe, P. R., Motsinger, R. E. & Sieckman, A. 1978 High velocity jet noise source location and reduction task 6 supplement-computer programs: engineering correlation (M*S) jet noise prediction method and unified aeroacoustic prediction model (M*G*B) for nozzles of arbitrary shape. *FAA-RD*-76-79, VIa.

Hu, T. F. & McLaughlin, D. K. 1990 Flow and acoustic properties of low Reynolds number underexpanded supersonic jets. *J. Sound Vib.* **141**, 485–405.

Hussain, F. & Husain, H. S. 1989 Elliptic jets. Part 1. Characteristics of unexcited and excited jets. *J. Fluid Mech.* **208**, 257–320.

Kantola, R. A. 1970 Noise characteristics of heated high velocity rectangular jets. *J. Sound Vib.* **64**, 277–294.

Kinzie, K. W. 1995 Aeroacoustic properties of moderate Reynolds number elliptic and rectangular supersonic jets. PhD Thesis, Penn State University.

Kinzie, K. W. & McLaughlin, D. K. 1997 Azimuthal mode measurements of elliptic jets. *Phys. Fluids* **9**, 2000–2008.

Kinzie, K. W. & McLaughlin, D. K. 1998 Measurements of supersonic helium air mixture jets. *AIAA/CEAS Paper* 98-2328.

Kovasznay, L. S. G. 1950 The hot-wire anemometer in supersonic flow. *J. Aero. Sci.* **17**, 565–584.

Lau, J. 1981 Effects of exit Mach number and temperature on mean-flow and turbulence characteristics in round jets. *J. Fluid Mech.* **105**, 193–218.

Lighthill, M. J. 1952 On sound generated aerodynamically. I. General theory. *Proc. R. Soc. Lond.* A **211**, 564–587.

Martens, S. 1995 Experiments in a compressible mixing layer. PhD thesis, The Pennsylvania State University.

Martens, S., Kinzie, K. W. & McLaughlin, D. K. 1994 Measurements of Kelvin–Helmholtz instabilities in a supersonic shear layer. *AIAA J.* **32**, 1633–1639.

McLaughlin, D. K., Barron, W. D. & Vaddempudi, A. R. 1992 Acoustic properties of supersonic helium/air jets at low Reynolds number. *DGLR/AIAA* 92-02-047.

McLaughlin, D. K., Morrison, G. L. & Troutt, T. R. 1975 Experiments on the instability waves in a supersonic jet and their acoustic radiation. *J. Fluid Mech.* **69**, 73–95.

Morris, P. J. & Bhat, T. R. S. 1992 The noise from supersonic elliptic jets. *DGLR/AIAA* 92-02-042.

Morris, P. J. & Bhat, T. R. S. 1993 Supersonic elliptic jet noise. *AIAA Paper* 93-4409.

Morris, P. J. & Bhat, T. R. S. 1995 The spatial stability of compressible elliptic jets. *Phys. Fluids* **7**, 185–194.

Morris, P. J. & Tam, C. K. W. 1979 On the radiation of sound by the instability waves of a compressible axisymmetric jet. In *Mechanisms of Sound Generation in Flows* (ed. E. A. Muller). Springer.

Morrison, G. L. & McLaughlin, D. K. 1979 Noise generation by instabilities in low Reynolds number supersonic jets. *J. Sound Vib.* **65**, 177–191.

Oster, D. & Wygnanski, I. 1982 The forced mixing layer between parallel streams. *J. Fluid Mech.* **123**, 91–130.

Schadow, K. C., Gutmark, E., Koshigoe, S. & Wilson, K. J. 1989 Combustion related shear-flow dynamics in elliptic supersonic jets. *AIAA J.* **27**, 1347–1353.

Seiner, J. M. 1992 Fluid dynamics and noise emission associated with supersonic jets. In *Studies in Turbulence* (ed. T. B. Gastski, S. Sutanu & C. G. Speziale), pp. 297–323. Springer.

Seiner, J. M., McLaughlin, D. K. & Liu, C. H. 1982 Supersonic jet noise generated by large scale instabilities. *NASA Tech. Paper* 2072.

Seiner, J. M. & Ponton, M. K 1991 Supersonic acoustic source mechanisms for free jets of various geometries. *AGARD 78thB Specialists Meeting on Combat Aircraft Noise, Bonn, Germany.*

Seiner, J. M., Ponton, M. K. Jansen, B. J. & Lagen, N. T. 1992 The effects of temperature on supersonic jet noise emission. *DGLR/AIAA* 92-02-046.

Stromberg, J. L., McLaughlin, D. K. & Troutt T. R. 1980 Flow field and acoustic properties of Mach number 0.9 jet at a low Reynolds number. *J. Sound Vib.* **72**, 159–176.

Tam, C. K. W. 1975 Supersonic jet noise generated by large scale disturbances. *J. Fluid Mech.* **38**, 51–79.

Tam, C. K. W. & Burton, D. E. 1984 Sound generated by instability waves of supersonic flows. Part 2. Axisymmetric jets. *J. Fluid Mech.* **138,** 273–295.

Tam, C. K. W. & Chen, P. 1994 Turbulent mixing noise from supersonic jets. *AIAA J.* **32**, 1774–1780.

Tam, C. K. W., Chen, P. & Seiner, J. M. 1992 Relationship between instability waves and noise of high-speed jets. *AIAA J.* **30**, 1747–1752.

Tam, C. K. W. & Morris, P. J. 1980 The radiation of sound by the instability waves of a compressible plane turbulent shear layer. *J. Fluid Mech.* **98**, 349–381.

Tanna, H. K., Dean, P. D. & Fisher, M. J. 1975 The influence of temperature on shock-free supersonic jet noise. *J. Sound Vib.* **39**, 429–460.

Troutt, T. R. & McLaughlin, D. K. 1982 Experiments on the flow and acoustic properties of a moderate Reynolds number supersonic jet. *J. Fluid Mech.* **116**, 123–156.

Winant, C. D. & Browand, F. K. 1974 Vortex pairing: the mechanism of turbulent mixing layer growth at moderate Reynolds number. *J. Fluid Mech.* **63**, 237–255.

Zaman, K. B. M. Q. 1995 Axis switching and spreading of an asymmetric jet – role of vorticity dynamics. *AIAA Paper* 95-0889.